2024 IEEE 63rd Conference on Decision and Control (CDC)
December 16-19, 2024. MiCo, Milan, Italy

Second-Order Newton-Based Extremum Seeking for Multivariable Static Maps

Azad Ghaffari
School of Engineering and Computing
Christopher Newport University
Newport News, VA, USA
azad.ghaffari@cnu.edu

Tiago Roux Oliveira
Dept. of Electronics and Telecommunication Engineering
State University of Rio de Janeiro
Rio de Janeiro, Brazil
tiagoroux@uerj.br

***Abstract*—A second-order Newton-based extremum seeking (SONES) algorithm is presented to estimate directional inflection points for multivariable static maps. The design extends the first-order Newton-based extremum seeking algorithm that drives the system toward its peak point. This work provides perturbation matrices to estimate the second- and third-order derivatives necessary for implementing the SONES. A set of conditions are provided for the probing frequencies that ensure accurate estimation of the derivatives. A differential Riccati filter calculates the inverse of the third-order derivative. The local stability of the new algorithm is proven for general multivariable static maps using averaging analysis. The proposed algorithm ensures uniform convergence toward directional inflection points without requiring information about the curvature of the map and its gradient. Simulation results show the effectiveness of the proposed algorithm.**

I. Introduction

A century since its invention and first application [1], and a quarter century since the proof of its convergence [2], extremum seeking (ES) is recognized as a valuable real-time optimization tool for model-free *dynamic* systems. Reference [3] highlights some of the ES principal advances in algorithm design, theory, and practical applications in several domains.

Confidence in ES, brought about by the proof of its stability for static and general nonlinear dynamic systems in continuous time [2], has engendered and accelerated the industrial uses of the ES. Examples include chip manufacturing, wind and photovoltaic energy, mobile robots, bioengineering systems, acoustic systems, noncooperative games, neuromuscular electrical stimulation, biological reactors, oil-drilling systems, and flow-traffic control for urban mobility. These engineering applications have been further enriched by recent theoretical developments that have opened the door to the design and analysis of new types of ES, such as those modeled by discrete-time systems [4], multivariable systems [5], non-cooperative games [6], hybrid dynamical systems [7], stochastic systems [8], [9], systems with delays [10], [11], and partial differential equations [12].

In particular, the authors of [5] present a multivariable Newton-based extremum seeking algorithm, which yields arbitrarily assignable convergence rates for each of the elements of the input vector. They generate the estimate of the Hessian matrix by generalizing the idea proposed in [13] for the scalar case. After that, Mills and Krstic [14] generalize the earlier results to a scalar version of the Newton-based extremum seeking algorithm which maximizes the map's high-order derivatives through measurements of the map. Hence, rather than optimizing the map itself, they offer a new scheme which can be useful in practice for maximizing the sensitivity of an input-to-output function to improve the signal-to-noise ratio as well as minimizing parameter sensitivity when designing feedforward controllers. For instance, the authors in [15] present a refrigeration system where a suitable operating point is located at the maximum negative slope that is subject to change. This point of zero curvature corresponds to a minimum of the first-order derivative of the input-output map. Hence, being able to track the minimum of the first-order derivative in real-time would allow the system to operate almost always at the most suitable operating condition. Following these ideas, Rusiti et al. [16] have expanded such domain application in order to include delays in the input and/or output channels of the maps to be optimized.

This paper considers the open problem of ES-based real-time optimization of the "first-order derivative" of multi-input maps, i.e., finding the extremum of the gradient vector of a multivariable static function. The term *high-order* ES encapsulates ES-based optimization at high-order derivatives. In general, $(n+1)^{\text{th}}$-order ES will optimize the n^{th}-order derivative. Following this notation, the conventional ES is "first-order," which optimizes the zeroth-order derivative (or the own function) for a given input-output map. Successful implementation of a second-order ES requires searching for zero columns of the Hessian matrix. On the other hand, a zero column of the Hessian matrix may indicate a directional inflection or saddle point. This work focuses on finding directional inflection points, where the curvature of the map changes direction. In addition, this problem has interesting aspects, such as the conditions that ensure the uniqueness of the gradient extremum point along all axes. Note that this work deals with vector spaces with increasing dimensions as the derivative order increases, leading to a new paradigm: the definition and estimation of extremum for vector functions.

This work focuses on estimating the directional inflection point via a perturbation-based ES, i.e., maximizing the gra-

dient along a priori known axis. In this event, if $y = h(\theta)$ with $\theta = [\theta_1 \ \theta_2 \ \cdots \ \theta_p]^\top$ has an inflection point along θ_m-axis, then the m^{th}-column of the Hessian matrix is zero, $\partial^2 h(\theta)/\partial\theta\partial\theta_m = 0$, and $\partial^3 h(\theta)/\partial^2\theta\partial\theta_m < 0$. A second-order gradient-based ES can be generated using Hessian's estimate to drive the system toward the inflection point. The curvature of the function heavily impacts the performance of gradient-based algorithms. One needs knowledge of the cost function curvature to properly tune the gradient-based algorithm, which becomes a complicated task in the case of multivariable maps. Therefore, this work proposes a second-order Newton-based ES (SONES), ensuring that the state trajectory uniformly converges toward a directional inflection point.

The SONES requires an accurate estimate of the second-order derivative and the inverse of the third-order derivative of the multivariable map. The inverse of the third-order derivative is produced by feeding the initial estimate of the third-order derivative to a dynamic Riccati filter. One challenging aspect of this work is producing the perturbation matrix that generates an accurate estimate of the third-order derivative. For this purpose, new conditions are obtained for the probing frequencies. Unlike [14], notice that such multiplicative dithers (or demodulation signals) are vectors rather than scalars for the multivariable case. The proposed perturbation matrix to estimate the Hessian of the map is a new variation of the matrix in [5]. A new perturbation matrix is presented to estimate the third-order derivative of the map. The number of conditions on the perturbation frequencies increases, but the proposed algorithm can successfully detect directional inflection points since the algorithm drives the system to the zero column of the Hessian. The proof utilizes the finite-horizon averaging theorem. Numerical simulations illustrate the obtained results.

Section II states the problem and presents the estimation of the second- and third-order derivatives. Section III presents the second-order Newton-based scheme and its stability analysis for the static map. Section IV presents an illustrative example to highlight the effectiveness of the SONES. Section V concludes the paper. Appendix A presents conditions on the probing frequencies.

II. High-Order Derivatives of Static Map

The conventional extremum seeking (ES) relies on driving the estimate of the gradient vector towards zero. Although the Newton-based ES removes the impact of the map curvature on the convergence rate of the algorithm, the gradient direction still determines the system convergence towards the extremum point. Therefore, in this work, the conventional gradient- and Newton-based algorithms are referred to as **first-order ES** algorithms, where the objective is to find the extremum value of an unknown map.

This work formulates an extremum seeking algorithm to estimate the directional inflection point of a multivariable static map. In other words, it is desirable to find the maximum gradient point along a priori known axis. Consider a differentiable static map of class $\mathcal{C}^r$ for $r \geq 3$

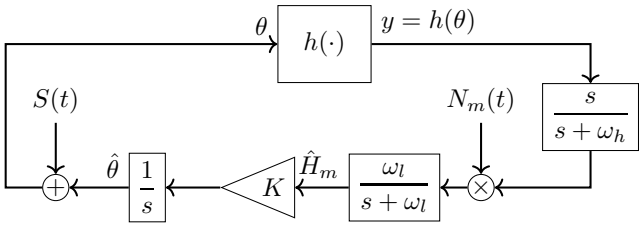

Fig. 1. Second-order gradient-based extremum seeking algorithm to find the directional inflection point along θ_m-axis, where K is a diagonal matrix with positive elements.

$$y = h(\theta), \quad \theta = \begin{bmatrix} \theta_1 & \theta_2 & \cdots & \theta_p \end{bmatrix}^\top. \tag{1}$$

The gradient vector of $y = h(\theta)$ is defined as

$$G(\theta) = [G_1(\theta) \ G_2(\theta) \ \cdots \ G_p(\theta)]^\top, \tag{2}$$

where $G_m(\theta) = \partial h(\theta)/\partial\theta_m$ for $m \in \{1, 2, \cdots, p\}$. Assume that $G_m(\theta)$ has a local maximum at θ^*, indicating that the curvature along θ_m-axis changes direction at θ^*. The inflection point corresponds to $\partial G_m(\theta)/\partial\theta = 0$, i.e., $\partial^2 h(\theta^*)/\partial\theta\partial\theta_m = 0$, meaning that the m^{th} column of the Hessian matrix is zero at the inflection point. The cost function is unknown in (1), but y can be measured and θ can be manipulated. Then, one can utilize prior work to estimate the Hessian and drive the system towards the inflection point. Therefore, the extremum seeking algorithm that determines the directional inflection point is called **second-order ES**.

Since the expansion of the gradient-based ES to estimate directional inflection points is straightforward, the details are left to the interested reader to explore. This work provides an algorithm and sketch of stability proof of a second-order Newton-based ES for static maps. The proposed algorithm requires the estimates of the second- and third-order derivatives along θ_m-axis.

The second-order gradient-based extremum seeking scheme for a multivariable static map is shown in Fig. 1, where K is a positive diagonal matrix, and the perturbation input is

$$S(t) = \begin{bmatrix} a_1 \sin(\omega_1 t) & \cdots & a_n \sin(\omega_n t) \end{bmatrix}^\top, \tag{3}$$

where $\omega_i \in \mathbb{R}$ and a_i's are small real numbers for $i \in \{1, 2, \cdots, p\}$. The estimate of column m of the Hessian matrix, $\hat{H}_m$, is the average of $N_m(t)y$. One can use (20) and (21) from [5] to generate $N_m(t)$. The probing frequencies need to satisfy

$$\omega_i \notin \Big\{\omega_j, \ \frac{1}{2}(\omega_j + \omega_k), \ \omega_j + 2\omega_k, \ \omega_j + \omega_k \pm \omega_l\Big\}, \tag{4}$$

for all distinct i, j, k, and l. The low- and high-pass filter is added to improve the accuracy of the estimate of column m of the Hessian matrix.

Although the prior work [5] provides the perturbation matrix to estimate the Hessian of a map, this research revisits the Hessian perturbation matrix to establish similar patterns between perturbation matrices to generate estimates of the first-, second-, and third-order derivatives of the map. Denote

$\tilde{\theta}=\hat{\theta}-\theta^*$. Using $\theta=\hat{\theta}+S(t)$, one obtains $\theta=\theta^*+\tilde{\theta}+S(t)$. Using the Taylor series expansion of the cost function around the inflection point gives

$$\begin{aligned}
y=&h(\theta^*+\tilde{\theta}+S(t))\\
=&h(\theta^*)+\sum_{i=1}^{p}\frac{\partial h(\theta^*)}{\partial\theta_i}\Big(\tilde{\theta}_i+S_i\Big)+\\
+&\frac{1}{2}\sum_{i=1}^{p}\sum_{j=1}^{p}\frac{\partial^2 h(\theta^*)}{\partial\theta_i\partial\theta_j}\Big(\tilde{\theta}_i+S_i\Big)\Big(\tilde{\theta}_j+S_j\Big)+\\
+&\frac{1}{6}\sum_{i=1}^{p}\sum_{j=1}^{p}\sum_{k=1}^{p}\frac{\partial^3 h(\theta^*)}{\partial\theta_i\partial\theta_j\partial\theta_k}\Big(\tilde{\theta}_i+S_i\Big)\Big(\tilde{\theta}_j+S_j\Big)\Big(\tilde{\theta}_k+S_k\Big)+\\
+&R(\tilde{\theta}+S(t)),
\end{aligned}\tag{5}$$

where $S_i=a_i\sin(\omega_i t)$ for $i\in\{1,2,\cdots,p\}$ and $R(\tilde{\theta}+S(t))$ stands for higher order terms in $\tilde{\theta}+S(t)$.

The average of the second-order derivative of (5) equals

$$\begin{aligned}
\frac{1}{\Pi}\int_0^{\Pi}\frac{\partial^2 y}{\partial\theta_i\partial\theta_j}\mathrm{d}t=&\frac{\partial^2 h(\theta^*)}{\partial\theta_i\partial\theta_j}+\sum_{k=1}^{p}\frac{\partial^3 h(\theta^*)}{\partial\theta_i\partial\theta_j\partial\theta_k}\tilde{\theta}_k+\\
&+\underbrace{\frac{1}{\Pi}\int_0^{\Pi}\frac{\partial^2 R(\tilde{\theta}+S(t))}{\partial\theta_i\partial\theta_j}\mathrm{d}t}_{O(|\tilde{\theta}|^2,|a|^2)},
\end{aligned}\tag{6}$$

where $i,j\in\{1,2,\cdots,p\}$, $O(z)\le M|z|$ for $|z|\le z_0$ and some positive M, and Π represents the averaging period. One can rewrite (5) as

$$\begin{aligned}
y=&\frac{1}{2}\sum_{i=1}^{p}\sum_{j=1}^{p}\left(\frac{\partial h(\theta^*)}{\partial\theta_i\partial\theta_j}+\sum_{k=1}^{p}\frac{\partial^3 h(\theta^*)}{\partial\theta_i\partial\theta_j\partial\theta_k}\tilde{\theta}_k\right)S_iS_j+\\
&+F(S_1,\cdots,S_p,S_1^3,\cdots,S_lS_mS_n,\cdots,S_p^3)+\\
&+R(\tilde{\theta}+S(t)),
\end{aligned}\tag{7}$$

where $F(\cdot)$ represents terms of the first- and third-order powers of the perturbation input $S(t)$. Note that

$$\sin(\omega_i t)\sin(\omega_j t)=\frac{1}{2}\Big(\cos(\omega_i-\omega_j)t-\cos(\omega_i+\omega_j)t\Big).\tag{8}$$

Then, one can generate an estimate of the second-order derivative by taking the average of $N(t)y$, where one option for the entries of $N(t)$ is as following

$$N_{i,i}=-\frac{8}{a_i^2}\cos(2\omega_i t)\tag{9}$$

$$N_{i,j}=-\frac{4}{a_ia_j}\cos(\omega_i+\omega_j)t,\quad i\neq j\tag{10}$$

for $i,j\in\{1,2,\cdots,p\}$. Proper choice of the probing frequencies will eliminate all the terms of $F(\cdot)N(t)$ in the average sense and gives

$$\begin{aligned}
\frac{1}{\Pi}\int_0^{\Pi}N_{i,j}(t)y\mathrm{d}t=&\frac{\partial^2 h(\theta^*)}{\partial\theta_i\partial\theta_j}+\sum_{k=1}^{p}\frac{\partial^3 h(\theta^*)}{\partial\theta_i\partial\theta_j\partial\theta_k}\tilde{\theta}_k+\\
&\underbrace{\frac{1}{\Pi}\int_0^{\Pi}R(\tilde{\theta}+S(t))N_{i,j}(t)\mathrm{d}t}_{O(|\tilde{\theta}|^2,|a|^2)}.
\end{aligned}\tag{11}$$

Comparing the right-hand side of (5) and (11) shows that the average of $N(t)y$ provides an accurate estimate of the second-order derivative of $y=h(\theta)$ in the average sense.

Following a similar approach, one can show that the average of the third-order derivative of the map gives

$$\begin{aligned}
\frac{1}{\Pi}\int_0^{\Pi}\frac{\partial^3 y}{\partial\theta_i\partial\theta_j\partial\theta_k}\mathrm{d}t=&\frac{\partial^3 h(\theta^*)}{\partial\theta_i\partial\theta_j\partial\theta_k}+\\
&+\underbrace{\frac{1}{\Pi}\int_0^{\Pi}\frac{\partial^3 R(\tilde{\theta}+S(t))}{\partial\theta_i\partial\theta_j\partial\theta_k}}_{O(|\tilde{\theta}|,|a|)}.
\end{aligned}\tag{12}$$

Moreover, (5) can be rewritten as

$$\begin{aligned}
y=&\frac{1}{6}\sum_{i=1}^{p}\sum_{j=1}^{p}\sum_{k=1}^{p}\frac{\partial^3 h(\theta^*)}{\partial\theta_i\partial\theta_j\partial\theta_k}S_iS_jS_k+\\
&+F'(S_1,\cdots,S_p,S_1^2,\cdots,S_p^2)+R(\tilde{\theta}+S(t)).
\end{aligned}\tag{13}$$

The following trigonometric identity holds

$$\begin{aligned}
\sin(\omega_i t)\sin(\omega_j t)\sin(\omega_k t)=&\frac{1}{4}\Big(\sin(\omega_i-\omega_j+\omega_k)t+\\
&+\sin(\omega_i+\omega_j-\omega_k)t-\sin(\omega_i-\omega_j-\omega_k)t-\\
&-\sin(\omega_i+\omega_j+\omega_k)t\Big).
\end{aligned}\tag{14}$$

An estimate of the third-order derivative of the map can be generated by taking the average of $P(t)y$, where one option for the entries of $P(t)$ is obtained as

$$P_{i,i,i}=-\frac{48}{a_i^3}\sin(3\omega_i t)\tag{15}$$

$$P_{i,i,j}=-\frac{16}{a_i^2a_j}\sin(2\omega_i+\omega_j)t,\quad i\neq j\tag{16}$$

$$P_{i,j,k}=-\frac{8}{a_ia_ja_k}\sin(\omega_i+\omega_j+\omega_k)t,\quad i\neq j\neq k,\tag{17}$$

for $i,j,k\in\{1,2,\cdots,p\}$. An appropriate choice of the probing frequencies will eliminate $F'(\cdot)P(t)$ in the average sense and provides

$$\begin{aligned}
\frac{1}{\Pi}\int_0^{\Pi}P_{i,j,k}(t)y\mathrm{d}t=&\frac{\partial^3 h(\theta^*)}{\partial\theta_i\partial\theta_j\partial\theta_k}+\\
&+\underbrace{\frac{1}{\Pi}\int_0^{\Pi}P_{i,j,k}(t)R(\tilde{\theta}+S(t))\mathrm{d}t}_{O(|\tilde{\theta}|,|a|)}.
\end{aligned}\tag{18}$$

Comparing the righ-hand side of (12) and (18) shows that the average of $P(t)y$ provides an accurate estimate of the third-order derivative of $y=h(\theta)$. The averaging period is obtained from

$$\Pi=2\pi\times\mathrm{LCM}\Big\{\frac{1}{\omega_i}\Big\},\quad i\in\{1,2,\cdots,p\},\tag{19}$$

where LCM stands for the least common multiple.

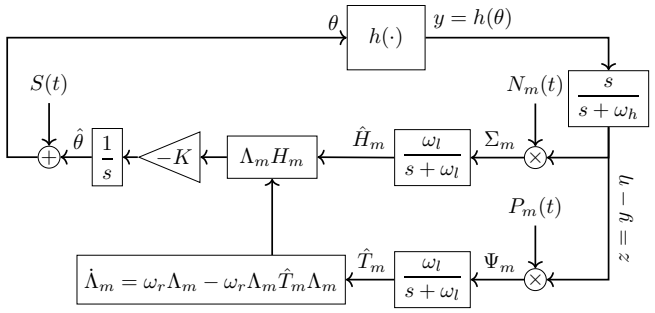

Fig. 2. Second-order Newton-based ES proposed for estimating the inflection point along θ_m-axis.

III. Second-Order Newton-Based ES

Consider a multivariable static map given by (1). The objective is to create a feedback mechanism which determines the directional inflection point of y without requiring the knowledge of either the inflection point, θ^*, or the functions $h(\cdot)$. Denote $H = \partial G(\theta)/\partial\theta = \partial^2 h(\theta)/\partial\theta^2$, where $G(\theta)$ is the gradient vector given by (2). Column m of matrix H is the gradient of $G_m(\theta)$, i.e., $H_m = \partial G_m(\theta)/\partial\theta$.

Assumption 1: There exists an inflection point θ^* along θ_m-axis that satisfies

$$\frac{\partial}{\partial\theta} G(\theta) = H, \quad H^\top = H \tag{20}$$

$$\frac{\partial}{\partial\theta} G_m(\theta^*) = H_m = 0 \tag{21}$$

$$\frac{\partial^2}{\partial\theta^2} G_m(\theta^*) = T_m < 0, \quad T_m^\top = T_m \tag{22}$$

Assumption 1 suggests that H_m vanishes at the inflection point. Hence, the estimate of H_m can be used to drive the system towards the inflection point using the gradient-based parameter update law shown in Fig. 1. The perturbation vector estimating H_m is given as

$$N_m(t) = -\frac{4}{a_m}\Big[\frac{\cos(\omega_1+\omega_m)t}{a_1}\cdots\frac{2\cos(2\omega_m)t}{a_m}\cdots \frac{\cos(\omega_p+\omega_m)t}{a_p}\Big]^\top. \tag{23}$$

The proof of stability of the second-order gradient-based algorithm is a straightforward expansion of the conventional (first-order) gradient-based ES.

Since a Newton-based adaptive law provides uniform transient and reduces control calibration efforts, this work proposes a second-order Newton-based ES for estimating directional inflection points. A block diagram of the algorithm is shown in Fig. 2. The perturbation vector $N_m(t)$ is given by (23) and perturbation matrix $P_m(t)$ is given as

$$P_m(t) = [P_{m,i,j}]_{p\times p}, \quad i,j \in \{1,2,\cdots,p\}, \tag{24}$$

where the entries are obtained from (15)–(17).

The probing frequencies ω_i's, the filter coefficients ω_h, ω_l, and ω_r and gain K are selected as

$$\omega_h = \delta\omega_h' = O(\delta) \tag{25}$$

$$\omega_l = \delta\omega_l' = O(\delta) \tag{26}$$

$$\omega_r = \delta\omega_r' = O(\delta) \tag{27}$$

$$K = \delta K'' = O(\delta), \tag{28}$$

where δ is a small positive constant, ω_i is a rational number, ω_h', ω_l', and ω_r' are $O(1)$ positive constants, and K' is a $p\times p$ diagonal matrix with $O(1)$ positive elements. Appendix A presents the conditions on the probing frequencies. Ignoring these conditions shifts the estimate of the parameter away from its true value, and leading to inaccurate estimates of the second- and third-order derivatives.

The system in Fig. 2 is summarized as

$$\frac{\mathrm{d}}{\mathrm{d}t}\left[\tilde{\theta}^\top \ \hat{H}_m^\top \ \tilde{\Lambda}_m \ \tilde{T}_m \ \tilde{\eta}\right]^\top = \begin{bmatrix} -K(\tilde{\Lambda}_m + T_m^{-1})\hat{H}_m \\ -\omega_l\hat{H}_m + \omega_l\Big(y - h(\theta^*) - \tilde{\eta}\Big)N_m(t) \\ \omega_r\left(\tilde{\Lambda}_m + T_m^{-1}\right)\Big(I - (\tilde{T}_m + T_m)(\tilde{\Lambda}_m + T_m^{-1})\Big) \\ -\omega_l\left(\tilde{T}_m + T_m\right) + \omega_l\Big(y - h(\theta^*) - \tilde{\eta}\Big)P_m(t) \\ -\omega_h\tilde{\eta} + \omega_h\Big(y - h(\theta^*)\Big) \end{bmatrix}, \tag{29}$$

where error variables are introduced as $\tilde{\theta} = \hat{\theta} - \theta^*$, $\tilde{\eta} = \eta - h(\theta^*)$, $\tilde{\Lambda}_m = \Lambda_m - T_m^{-1}$, and $\tilde{T}_m = \hat{T}_m - T_m$, and $\theta = \hat{\theta} + S(t)$. A slight abuse of notation is performed by stacking matrix quantities $\tilde{\Lambda}_m$ and $\tilde{T}_m$ along with vector quantities, as alternative notational choices would be more cumbersome.

The average system is obtained as

$$\frac{\mathrm{d}}{\mathrm{d}t}\left[\tilde{\theta}^{\mathrm{a}\top} \quad \hat{H}_m^{\mathrm{a}\top} \quad \tilde{\Lambda}_m^{\mathrm{a}} \quad \tilde{T}_m^{\mathrm{a}} \quad \tilde{\eta}^{\mathrm{a}}\right]^\top = \delta\begin{bmatrix} -K'(\tilde{\Lambda}_m^{\mathrm{a}} + T_m^{-1})\hat{H}_m^{\mathrm{a}} \\ -\omega_l'\hat{H}_m^{\mathrm{a}} + \omega_l'\frac{1}{\Pi}\int_0^\Pi \nu(\tilde{\theta}^{\mathrm{a}} + S(t))N_m(t)\mathrm{d}t \\ \omega_r'(\tilde{\Lambda}_m^{\mathrm{a}} + T_m^{-1})\big(I + (\tilde{T}_m^{\mathrm{a}} + T_m)(\tilde{\Lambda}_m^{\mathrm{a}} + T_m^{-1})\big) \\ -\omega_l'(\tilde{T}_m^{\mathrm{a}} + T_m) + \omega_l''\frac{1}{\Pi}\int_0^\Pi \nu(\tilde{\theta}^{\mathrm{a}} + S(t))P_m(t)\mathrm{d}t \\ -\omega_h'\tilde{\eta}^{\mathrm{a}} + \omega_h'\frac{1}{\Pi}\int_0^\Pi \nu(\tilde{\theta}^{\mathrm{a}} + S(t))\mathrm{d}t \end{bmatrix}, \tag{30}$$

where $\nu(q) = h(\theta^* + q) - h(\theta^*)$. In view of Assumption 1, $\partial^2\nu(0)/\partial q\partial q_m = 0$, $\partial^3\nu(0)/\partial q^2\partial q_m = T_m < 0$. The stability of the average system is summarized in the following theorem.

Theorem 1: Consider system (30) under Assumption 1. There exist $\bar{\delta}, \bar{a} > 0$ such that for all $\delta \in (0, \bar{\delta})$ and $|a| \in (0, \bar{a})$ system (30) has a unique exponentially stable periodic solution $\big(\tilde{\theta}^\Pi(t), \hat{H}_m^\Pi(t), \tilde{\Lambda}_m^\Pi(t), \tilde{T}_m^\Pi(t), \tilde{\eta}^\Pi(t)\big)$ of period Π and this solution satisfies

$$\left|\tilde{\theta}_i^\Pi(t) - \sum_{j=1}^p c_j^i a_j^2\right| \le O(\delta + |a|^3), \tag{31}$$

$$\left|\hat{H}_m^\Pi(t)\right| \le O(\delta), \tag{32}$$

$$\left|\tilde{T}_m^\Pi(t)\right| \le O(\delta + |a|^2), \tag{33}$$

$$\Big|\tilde{\eta}^{\Pi}(\tau)-\sum_{i=1}^{p}\frac{\partial\nu(0)}{\partial q_i}\sum_{j=1}^{p}c_j^i a_j^2-,$$
$$-\frac{1}{4}\sum_{i=1}^{p}\frac{\partial^2\nu(0)}{\partial q_i^2}a_i^2\Big|\leq O(\delta+|a|^4), \quad (34)$$
$$\big(\tilde{T}_m^{\Pi}(t)+T_m\big)\big(\tilde{\Lambda}_m^{\Pi}(t)+T_m^{-1}\big)=I \quad (35)$$

for all $t\geq 0$, where

$$\big[\,c_j^1\;\;c_j^2\;\;\cdots\;\;c_j^p\,\big]^{\top}=-\frac{1}{2}T_m^{-1}\frac{\partial^4}{\partial q\partial q_j^2\partial q_m}\nu(0) \quad (36)$$

for all $i,j\in\{1,2,\cdots,p\}$.

Note that $\bullet^{\Pi}$ and $\bullet^{\mathrm{a}}$ represent a periodic variable and its average, respectively. Proof of Theorem 1 is omitted due to space constraints. The following provides a sketch for the proof. The Jacobian matrix of the averaged system (30) at the equilibrium point is obtained as

$$J^{\mathrm{a,e}}=\delta\begin{bmatrix}A_{1,1} & 0_{2p\times(2p+1)}\\ A_{2,1} & A_{2,2}\end{bmatrix}, \quad (37)$$

where the states are split as $[\tilde{\theta}^{\mathrm{a}\top}\hat{H}_m^{\mathrm{a}\top}]^{\top}$ and $[\tilde{\Lambda}_m\;\tilde{T}_m\;\tilde{\eta}]^{\top}$. $A_{2,2}$ is Hurwitz and one can show that

$$A_{1,1}=\begin{bmatrix}0_{p\times p} & -K'\big(\tilde{\Lambda}_m^{\mathrm{a}}+T_m^{-1}\big)\\ \frac{\omega_l'}{\Pi}\int_0^{\Pi}\frac{\partial\nu}{\partial q}N_m\mathrm{d}t & -\omega_l' I_{p\times p}\end{bmatrix} \quad (38)$$

is Hurwitz for small $|a|$. Since $J^{\mathrm{a,e}}$ is lower-triangular and $A_{1,1}$ and $A_{2,2}$ are Hurwitz, then $J^{\mathrm{a,e}}$ is Hurwitz and the equilibrium of the average system (30) is exponentially stable if all elements of vector a are sufficiently small. The proof can be completed using the averaging theorem [17]. The stability result is local.

IV. Simulation Results

To illustrate the results and highlight the effectiveness of the second-order Newton-based extremum seeking method, the following static input-output map is considered

$$\begin{aligned}y=&h(\theta)\\ =&1+(\theta_1-\theta_1^*)-1*(\theta_2-\theta_2^*)+\frac{3}{2}(\theta_2-\theta_2^*)^2-\\ &-\frac{1}{6}\Big(2(\theta_1-\theta_1^*)^3+3(\theta_1-\theta_1^*)^2(\theta_2-\theta_2^*)+\\ &+12(\theta_1-\theta_1^*)(\theta_2-\theta_2^*)^2+(\theta_2-\theta_2^*)^3\Big),\end{aligned} \quad (39)$$

where $\theta^*=[1\;\;2]^{\top}$. The map has an inflection point along θ_1-axis at θ^*, i.e., $G_1(\theta)=\partial h(\theta)/\partial\theta_1$ has a maximum at θ^*, which in turn leads to $H_1=\partial^2 h(\theta^*)/\partial\theta\partial\theta_1=0$ and

$$T_1=\frac{\partial^3}{\partial^2\theta\partial\theta_1}h(\theta^*)=\begin{bmatrix}-2 & -1\\ -1 & -4\end{bmatrix}<0 \quad (40)$$
$$\Lambda_1=T_1^{-1}=\begin{bmatrix}-0.57 & 0.14\\ 0.14 & -0.29\end{bmatrix}. \quad (41)$$

The test is performed with the following parameters, $\omega=[500\;\;300]^{\top}$ rad/s, $\omega_h=\omega_l=\omega_r=1$ rad/s, $a=[0.1\;\;0.1]^{\top}$, $K=\mathrm{diag}([0.02\;\;0.02])$, $T_1(0)=\mathrm{diag}([-50\;\;-50])$, $\Lambda_1(0)=T_1(0)^{-1}$, $\theta_0=[0\;\;0]^{\top}$. Note that $T_1(0)$ is a diagonal matrix with entries of large absolute values to avoid numerical singularities during the transient.

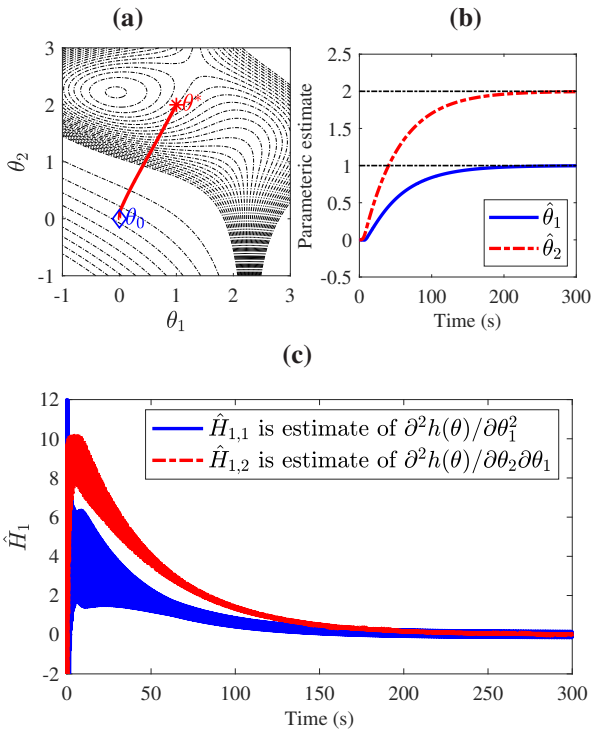

Fig. 3. (a) The second-order Newton-based ES algorithm governs the system trajectory toward the inflection point along θ_1-axis at $\theta^*=[1\;\;2]^{\top}$. The level sets of $y=h(\theta)$ indicate that the inflection point is near a local minimum point and a saddle point at $[-0.07\;\;2.22]^{\top}$ and $[1.26\;\;2.62]^{\top}$, respectively. (b) The estimate of the parameters versus time. Please note the uniform transient of the parameters. (c) Temporal evolution of the second-order derivative that drives the system toward the inflection point along θ_1-axis.

The inflection point is near a local minimum and saddle point that are respectively located at $[-0.07\;\;2.22]^{\top}$ and $[1.26\;\;2.62]^{\top}$. Fig. 3(a) illustrates the system trajectory among the level sets of the map. The algorithm successfully drives the system toward the inflection point as verified by Fig. 3(c), showing that the first column of the Hessian moves toward zero. Fig. 3(b) shows the evolution of the parameters versus time. Fig. 4(a) shows that the algorithm maximizes the gradient along θ_1-axis. Fig. 4(b) shows that the gradient along θ_2-axis has a saddle point at $[1.8\;\;1.8]^{\top}$. Fig. 5 verifies that Λ_1 converges to its actual value under 15 seconds despite large initialization error. Generally, it is advised to set $T_1(0)$ such that $\Lambda_1(0)$ has small entries so that the algorithm can cope with large transients that may otherwise destabilize the system.

V. Conclusions

The directional inflection points of multivariable static maps can be estimated using a second-order gradient-based extremum seeking algorithm. However, the gradient-based estimation algorithms rely on the cost function curvature, which may lead to low transient performances, especially when the cost function is the derivative of another function.

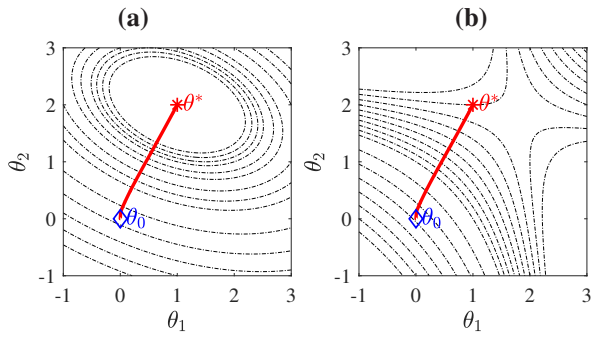

Fig. 4. (a) System trajectory among level sets of $G_1(\theta) = \partial h(\theta)/\partial\theta_1$. The inflection point along θ_1-axis corresponds to the maximum of $G_1(\theta)$. (b) System trajectory among level sets of $G_2 = \partial h(\theta)/\partial\theta_2$ indicating a saddle point.

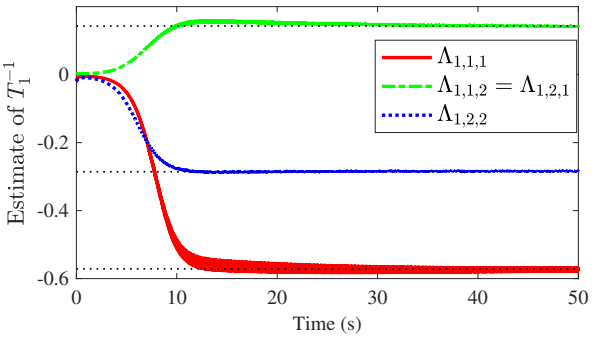

Fig. 5. Temporal evolution of the estimate of the third-order derivative. The true value of Λ_1 is reached under 15 seconds.

As the number of parameters grows, achieving a uniform convergence rate of all parameters by tuning the estimation gain will become cumbersome. The Newton-based algorithm, which relies on the estimation of two consecutive derivatives at the same time, removes the trial and error process to update all parameters uniformly and facilitates a user-assignable convergence rate. Properly choosing probing frequencies and carefully selecting corner frequencies of the high-pass, low-pass, and Riccati filters ensures accurate estimation of the second-order derivative and the inverse of the third-order derivative. Future work will expand the SONES algorithm to dynamic maps and improve its convergence rate by utilizing high-order low-pass filters.

Appendix A
Conditions on Probing Frequencies

The following conditions must be met for the probing frequencies to obtain an accurate estimate of the second- and third-order derivatives of the map.

$$
\begin{aligned}
&\omega_i \in \Omega \text{ for } i = 1, 2, \cdots, p \qquad (42)\\
&\Omega = \{\omega_i \in \mathbb{R}_{>0} \mid \\
&\quad \omega_i \neq \omega_j \wedge \omega_i \neq 2\omega_j \wedge \omega_i \neq 3\omega_j \wedge \omega_i \neq 5\omega_j \wedge \\
&\quad \omega_i \neq \omega_j + \omega_k \wedge \omega_i \neq \omega_j + \omega_k + \omega_l \wedge \\
&\quad \omega_i \neq \omega_j + 2\omega_k \wedge \omega_i \neq \omega_j + 4\omega_k \wedge \\
&\quad \omega_i \neq 2\omega_j + 3\omega_k \wedge \\
&\quad \omega_i \neq \omega_j + 2\omega_k + 2\omega_l \wedge \omega_i \neq \omega_j + \omega_k + 3\omega_l \wedge \\
&\quad \omega_i \neq \omega_j + \omega_k + \omega_l + 2\omega_m \wedge \\
&\quad \omega_i \neq \omega_j + \omega_k + \omega_l + \omega_m + \omega_n \wedge \\
&\quad \omega_i \neq \frac{\omega_j + \omega_k}{2} \wedge \omega_i \neq \frac{\omega_j + 3\omega_k}{2} \wedge \\
&\quad \omega_i \neq \frac{\omega_j + 2\omega_k}{3} \wedge \omega_i \neq \frac{\omega_j + \omega_k + \omega_l}{3} \wedge \\
&\quad \omega_i \neq \frac{\omega_j + \omega_k}{4} \wedge \omega_i \neq \frac{\omega_j + \omega_k + 2\omega_l}{2} \wedge \\
&\quad \omega_i \neq \frac{\omega_j + \omega_k + \omega_l + \omega_m}{2} \wedge \\
&\quad \omega_i + \omega_j \neq \omega_k + \omega_l \wedge \omega_i + \omega_j \neq \omega_k + 3\omega_l \wedge \\
&\quad \omega_i + \omega_j \neq 2\omega_k + 2\omega_l \wedge \omega_i + \omega_j \neq \omega_k + \omega_l + 2\omega_m \wedge \\
&\quad \omega_i + \omega_j \neq \omega_k + \omega_l + \omega_m + \omega_n \wedge \\
&\quad \omega_i + 2\omega_j \neq \omega_k + 2\omega_l \wedge \omega_i + 2\omega_j \neq \omega_k + \omega_l + \omega_m \wedge \\
&\quad \omega_i + \omega_j + \omega_k \neq \omega_l + \omega_m + \omega_n \\
&\quad \forall i \neq j \neq k \neq l \neq m \neq n \in \{1, 2, \cdots, p\}\}
\end{aligned}
$$

References

[1] M. Leblanc, Sur l'électrification des chemins de fer au moyen de courants alternatifs de fréquence élevée, *Revue Générale de l'Electricité*, vol. XII, pp. 275–277, 1922.

[2] M. Krstic and H. H. Wang, Stability of extremum seeking feedback for general dynamic systems, Automatica, vol. 36, pp. 595-601, 2000.

[3] A. Scheinker, 100 years of extremum seeking: A survey, Automatica, vol. 161, 111481, 2024.

[4] J.-Y. Choi, M. Krstić, K. B. Ariyur, and J. S. Lee, Extremum seeking control for discrete-time systems, *IEEE Trans. Automat. Contr.*, vol. 47, pp. 318–323, 2002.

[5] A. Ghaffari, M. Krstić, and D. Nešic, Multivariable Newton-based extremum seeking, *Automatica*, vol. 48, pp. 1759–1767, 2012.

[6] P. Frihauf, M. Krstic, and T. Başar, Nash equilibrium seeking in noncooperative games, IEEE Transactions on Automatic Control, vol. 57, pp. 1192-1207, 2012.

[7] J. I. Poveda and A. R. Teel. A framework for a class of hybrid extremum seeking controllers with dynamic inclusions, *Automatica*, vol. 76,pp. 13–126, 2017.

[8] C. Manzie and M. Krstić, Extremum seeking with stochastic perturbations, *IEEE Trans. Automat. Contr.*, vol. 54, pp. 580–585, 2009.

[9] S.-J. Liu and M. Krstić, Stochastic averaging in continuous time and its applications to extremum seeking, *IEEE Trans. Automat. Contr.*, vol. 55, pp. 2235–2250, 2010.

[10] T. R. Oliveira, M. Krstić, and D. Tsubakino, Extremum seeking for static maps with delays, *IEEE Trans. Automat. Contr.*, vol. 62, pp. 1911–1926, 2017.

[11] Y. Zhu, E. Fridman, and T. R. Oliveira, Sampled-data extremum seeking with constant delay: a time-delay approach, *IEEE Trans. Automat. Contr.*, vol. 68, pp. 432–439, 2023.

[12] T. R. Oliveira and M. Krstic, *Extremum Seeking through Delays and PDEs*, SIAM, 2022.

[13] D. Nešic, Y. Tan, W. H. Moase, and C. Manzie, A unifying approach to extremum seeking: adaptive schemes based on the estimation of derivatives, In Proc. of IEEE conf. on decision and control, pp.4625–4630, Atlanta, USA, 2010

[14] G. Mills and M. Krstić, Maximizing map sensitivity and higher derivatives via extremum seeking, *IEEE Trans. Automat. Contr.*, vol. 63, pp. 3232–3247, 2018.

[15] K. Vinther, H. Rasmussen, R. Izadi-Zamanabadi, and J. Stoustrup,, Single temperature sensor superheat control using a novel maximum slope-seeking method, *International Journal of Refrigeration*, vol. 36, pp. 1118–1129, 2013.

[16] D. Rusiti, T. R. Oliveira, G. Mills, and M. Krstić, Deterministic and stochastic Newton-based extremum seeking for higher derivatives of unknown maps with delays, *European Journal of Control*, vol. 41, pp. 72–83, 2018.

[17] H. K. Khalil, *Nonlinear systems (2nd ed.),* Prentice Hall, 1996.